TECHNICAL UNIVERSITY OF CLUJ-NAPOCA

ACTA TECHNICA NAPOCENSIS

Series: Applied Mathematics, Mechanics, and Engineering
Vol. 64, Issue III, September, 2021

NUMERICAL SOLUTION OF ENGINEERING PROBLEMS REGARDING ELASTIC TIGHTENING JOINTS

Cristian – Ioan INOAN, Radu – Nicolae CORCHEȘ, Gheorghina RUS, Gheorghe ACHIMAȘ

ABSTRACT: The finite element method is currently the most widespread process for numerically solving engineering problems. When applying MEF, the domain occupied by the physical system under analysis is discretized into finite-sized subdomains bounded by rectilinear or curvilinear boundaries. Through this operation, the real system is replaced by a network of so-called finite elements.

By applying MEF we obtain a system of equations that is solved numerically in relation to the values of the unknown knots. The main advantages of MEF are the following: flexibility (by allowing the discretization of bodies of any complex shape); the possibility to model inhomogeneous bodies from the point of view of physical properties; easy implementation in general computer programs. The most important disadvantage of MEF is the large volume of input data required for the construction and numerical solving of the model.
***KEYWORDS*:** finite elements, MEF, types of finite elements.

1. INTRODUCTION

Currently, the finite element method is widely used in the field of computer aided design of shrinkage assemblies. The Abaqus/Standard finite element analysis program [Aba2011a, Aba2011b, Aba2011c] was chosen for the numerical simulation of the shrinkage process at room temperature. From the benefits of using this program, the most important are the following:

- the existence of a graphic pre-processor (Abaqus/CAE), through which the finite element model of the analyzed process can be easily generated;
- facilities for importing geometric patterns in various formats recognized by design programs (e.g. IGES, STEP, DXF, etc.);
- flexibility in the mechanics of the process under analysis thanks to the "step" decomposition mechanism;
- the availability of a wide range of constitutive models as well as realistic models of rubbing contact;
- the existence of a very diverse library of finite elements;
- the existence of a module for the automatic discretization of geometric models;
- the existence of a post-processor (Abaqus/Viewer) that provides graphical representations of the simulation results (in the case of shrinkage processes, the distribution of stresses in the assembled parts are useful, as well as the diagram describing the variation of the pressing force).

The layout of the shrinkage assembly that is the object of the analysis is presented in figure 1. The process is considered to take place at the room temperature and involves the forced insertion of hub 4 into the bore of part 2. The latter is centered at both ends by means of rings 1 and 3. Ring 1 also serves to support the whole assembly on the table of a press. The slider of the press exerts a pressure on the upper head of the hub 4, forcing its entry into the bore of part 2. The nominal diameters of the cylindrical surfaces on which the shrinking is performed have the following values: 57,6 mm in the case of the hub 4, respectively 57,5 mm in case of the bore in the part

2 (resulting in a nominal tightening of 0.1 mm). The parts shown in figure 1 are made of the following materials: alloy tool steel X210CrW12 (SR EN ISO 4957: 2018) in the case of part 2 and hub 4, respectively non-alloy steel for hardening and tempering C45 (SR EN 10083-2: 2007) in the case of rings 1 and 3.

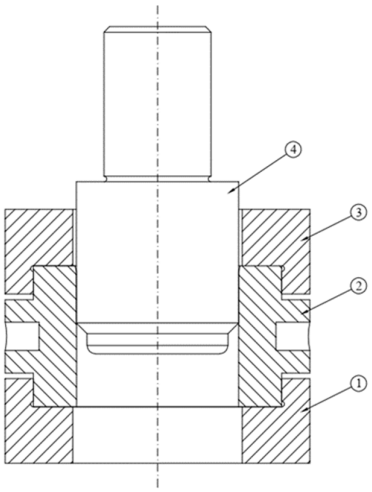

Fig. 1. Layout of the shrink assembly that is the object of the analysis with finite elements (1 - support ring; 2 - pressing ring; 3 - centering ring; 4 - pressing hub)

The finite element analysis of the shrinkage process was performed adopting the hypothesis of an elastic behavior of all parts presented in figure 1. Table 1 shows the elastic parameters of the two steels from which the respective parts are made (Young's modulus, respectively the Poisson's ratio).

Table 1. The elastic parameters of the steel used for the execution of the shrinkage assembly parts from the figure 1.

Steel grade	Young's modulus [MPa]	Poisson's ratio [-]
X210CrW12	220000	0.3
C45	210000	0.3

The Abaqus/Standard program shapes the contact between bodies using a penalty function. The bodies that are part of the finite element model are divided into two categories: "masters" – more resistant bodies or rigid bodies, respectively "slaves" – easier deformable bodies.

The contact algorithm detects the tendency of the knots belonging to the "slave" bodies to penetrate through the borders of the "master" bodies. When a penetration is encountered, a repulsive force is applied to the knots of the "slave" body, which tends to bring them to the surface of the "master" body. The repulsive force has both a normal component on the surface of the "master" body and a tangential component. The normal part is defined by a penalty function. As for the tangential component, it is essentially a Coulomb friction law, in the structure of which the coefficient μ intervenes.

In the case of the shrink assembly in figure 1, a friction coefficient $\mu = 0.125$ was adopted on the surfaces of the bodies between which there are very little or no relative displacements. As for the bodies between which there are relatively large displacements (part 2 and hub 4), various values of the coefficient μ have been adopted on their contact surfaces: 0.075; 0.100; 0.125; 0.150; 0.175. For each of these values, a distinct analysis of the shrinkage process was performed, thus aiming to simulate the most diversified lubrication conditions.

2. FINITE ELEMENT ANALYSIS OF THE SHRINKAGE PROCESS

In the following will be detailed the stages of the finite element analysis of the shrinkage process shown schematically in figure 1.

1. Importing the geometric representations of the parts that are part of the finite element model of the shrinkage process – figure 2.

Remarks:

- Geometric representations were developed using the SolidWorks design program, being transferred to the Abaqus/CAE pre-processor via STEP files.
- Along with the parts from figure 1, in the finite element model of the shrinkage process was also introduced the representation of the working surface of a turntable (position 5 in figure 2). The turntable will force the insertion of the hub 4 into the bore of the part 5.

- As can be seen in Figure 2, taking advantage of the symmetry of components 1, 2, 3 and 4 in relation to two mutually perpendicular planes, the representations of these components were reduced to a quarter of the actual geometry. Obviously, the surfaces resulting from the sectioning with the axial planes will receive boundary conditions likely to reflect the mechanical action of the portions removed from the model, namely, the blocking of translations along the normal line to the axial planes and blocking the rotations around the symmetry axis enclosed in the respective plane.

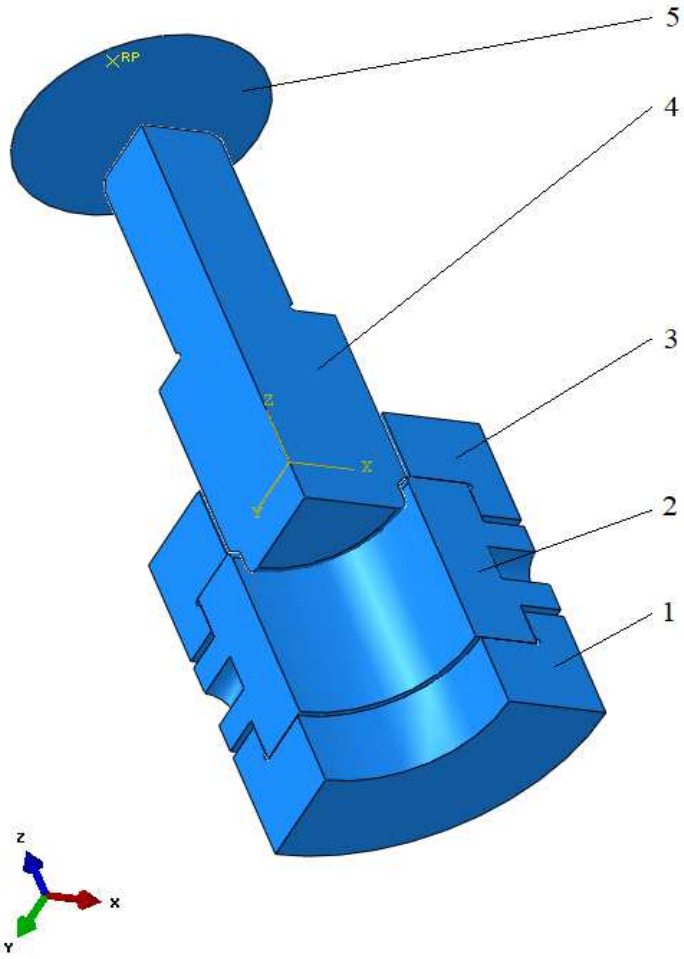

Fig. 2. Geometrical representations of the parts that make up the finite element model of the shrinkage process (1 – support ring; 2 – pressing ring; 3 – centering ring; 4 – pressing hub; 5 –work surface of the turntable)

With the import of geometric representations, their status was defined (deformable or rigid): deformable bodies in the case of components 1, 2, 3, 4 and 5, respectively rigid surface in the case of component 5.

2. Description of the elastic behavior of the deformable bodies included in the finite element model of the shrinkage process (see table 1, respectively figures 3 and 4)

3. Defining the shrinkage process as an analysis step (fig. xx.5)

4. Definition of the parameters describing the frictional contact between the components of the finite element model (see the explanations at the end of § 1, respectively figures 6 and 7)

5. Selection of the pairs of "master" - "slave" entities that may come into contact during the analyzed shrinkage process (see figure xx.8 and table xx.2)

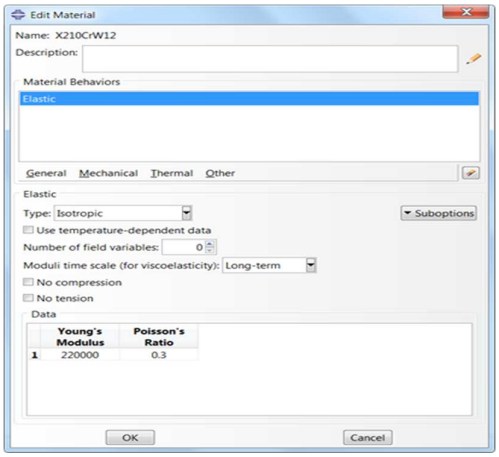

Fig. 3. Definition of the elastic characteristics of steel X210CrW12 - the basic material of components 2 and 4 (see data in table 1)

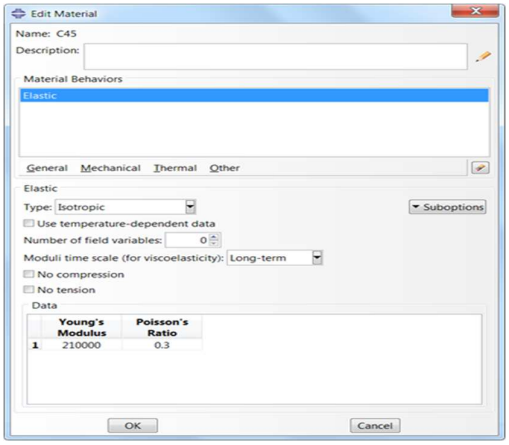

Fig. 4 Definition of the elastic characteristics of C45 steel – the basic material of components 1 and 3 (see data in table 1)

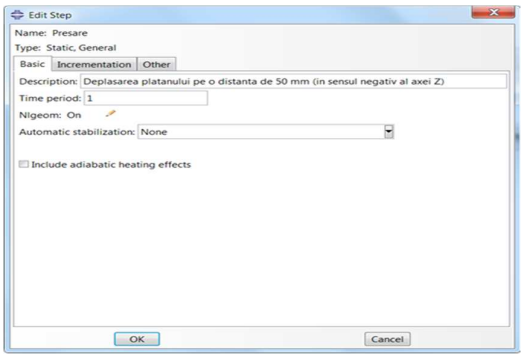

Fig. 5. Definition of the shrinkage process as a stage of analysis

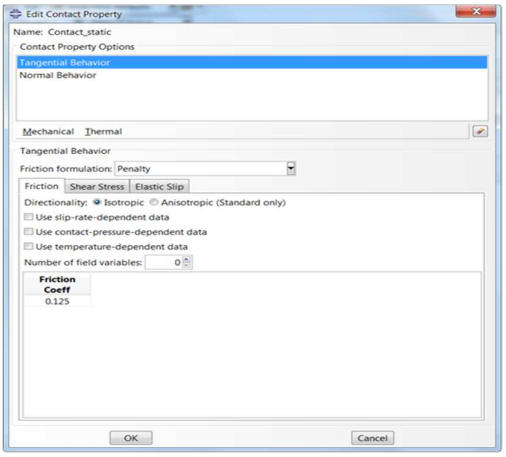

Fig. 6. Definition of the friction coefficient to be associated with the contact surfaces of bodies between which there are very little or no relative displacements (see also the explanations at the end § 1)

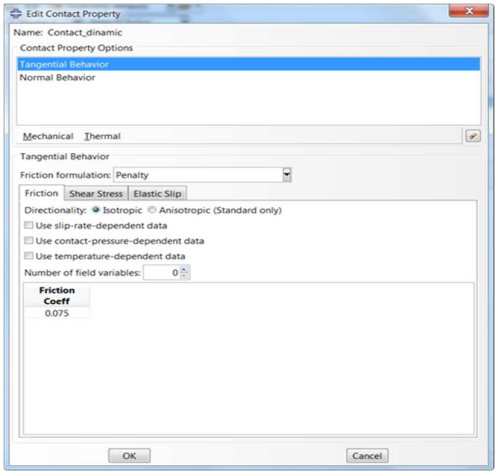

Fig. 7. Definition of the friction coefficient to be associated with the contact surfaces of bodies between which there are relatively large displacements (see also the explanations at the end § 1)

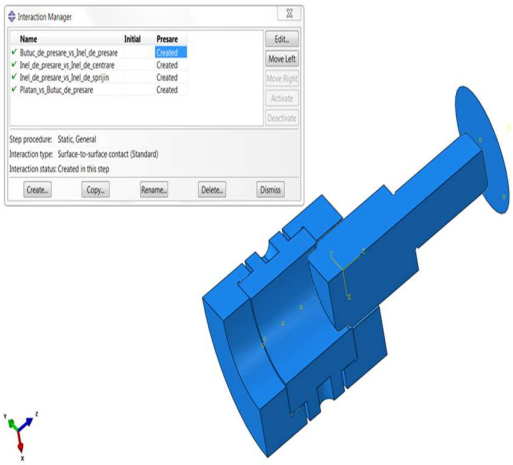

Fig. 8. Pairs of "master" - "slave" entities that may come into contact during the analyzed shrinkage process (see also details in the table 2)

Table 2.
Friction coefficients μ associated with the pairs of “master” - “slave” entities that may come into contact during the analyzed shrinkage process (see figure 2 and explanations at the end § 1.

“Master” entity	“Slave” entity	Friction coefficient μ [-]
Pressing hub 4	Pressing ring 2	0,075 0,100 0,125 0,150

		0,175
Pressing ring 2	Centering ring 3	0,125
Pressing ring 2	Support ring 1	0,125
Turntable 5	Pressing hub 4	0,125

6. Specifying the boundary conditions that define the analyzed shrinkage process under kinematic aspect (see figures 9 and 10)

Remarks:

- Kinematic restrictions introduce constraints of the degrees of freedom for one or another of the components of the finite element model. In the case of the turntable (rigid surface), these constraints are introduced on the associated reference point. For deformable components of the finite element model, the kinematic restrictions apply to the degrees of nodal freedom.

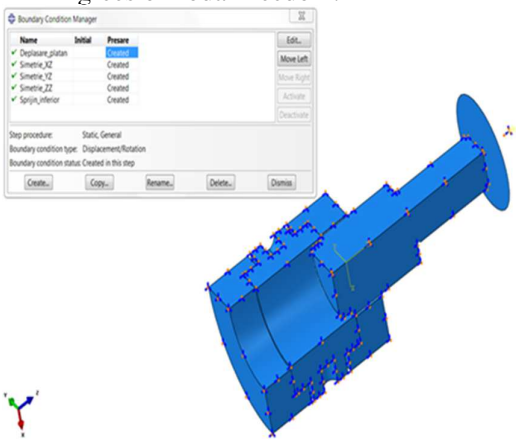

Fig. 9. Boundary conditions that define the analyzed shrinkage process under kinematic aspect.

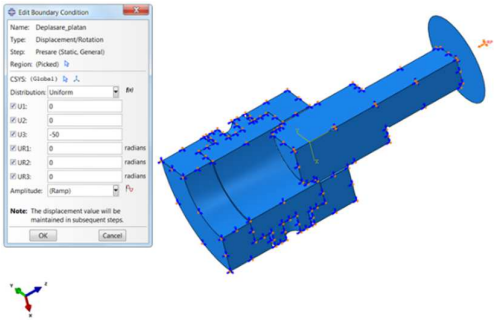

Fig. 10. Imposing the movement of the turntable over a distance of 50 mm in the negative direction of the axis Oz.

- The symmetry of the deformable components of the finite element model in relation to the Oxz and Oyz planes imposes the introduction of appropriate kinematic restrictions, namely, the prohibition of translation along the normal lines to these planes, as well as of rotations around the coordinate axes contained in those planes.
- Supporting the entire shrinkage assembly on the press table is modeled by locking the translation along the Oz axis for the knots on the lower surface of the support ring 1.
- The forced insertion of the hub 4 into the bore of the workpiece 2 is achieved by forcing the movement of the turntable 5 over a distance of 50 mm, in the negative direction of the Oz axis. This kinematic restriction is applied to the reference point associated with the turntable (fig. 10)

7. Discretization of the components that form the finite element model of the shrinkage process (fig. 11)

Remarks:

- The deformable components of the model were discretized using second-order tetrahedral finite elements (with six knots).
- The rigid surface of the turntable was discretized using first order triangular finite elements (with three knots).

8. Launch of the Abaqus/Standard program to solve the finite element model of the shrinkage process

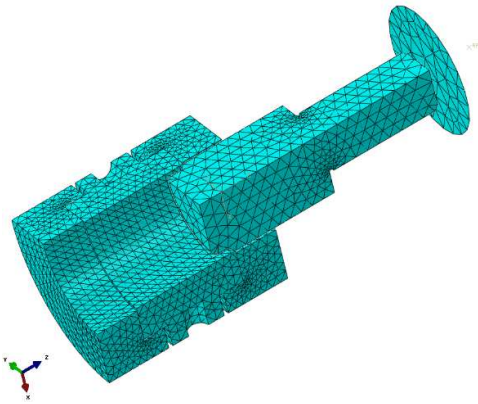

Fig. 11. Discretization of the components that form the finite element model of the shrinkage process

9. Analysis and interpretation of numerical results using the Abaqus/Viewer post-processor

Of the information provided by the Abaqus / Viewer post-processor, the most important are the following:

- the distribution of the equivalent von Mises stress at the level of the parts that form the shrinkage assembly (fig. 12, 13, 14, 15 and 16);
- the evolution of the pressing force developed by the turntable 5 depending on the axial displacement of the hub 4 (fig. 17).

Figures 12, 13, 14, 15 and 16 show the distribution of the equivalent von Mises stress in the final stage of the assembly process, for different values of the friction coefficient associated with the contact surface between the hub 4 and the part 2. As expected, the increase in the friction coefficient causes higher and higher values of the maximum stress. The stress distributions obtained by finite element analysis show that, regardless of the level of friction, part 2 is more stressed than hub 4.

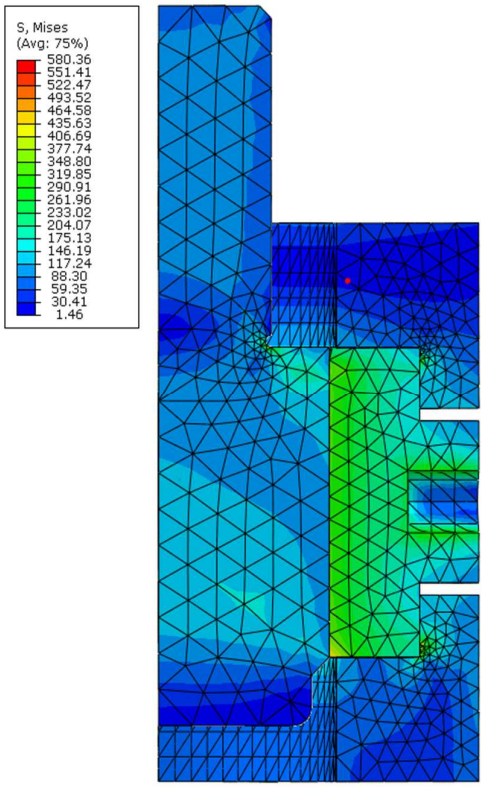

Fig. 12. Distribution of the equivalent von Mises stress at the level of the parts that make up the shrinkage assembly at an axial displacement of the hub of 50 mm (in the case of a friction coefficient $\mu = 0.075$ on the contact surface between the hub 4 and part 2)

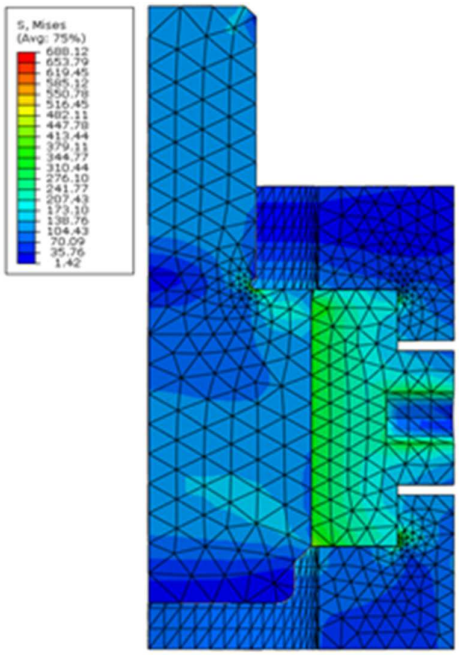

Fig. 13. Distribution of the equivalent von Mises stress at the level of the parts that make up the shrinkage assembly at an axial displacement of the hub of 50 mm (in the case of a friction coefficient $\mu = 0.100$ on the contact surface between the hub 4 and part 2)

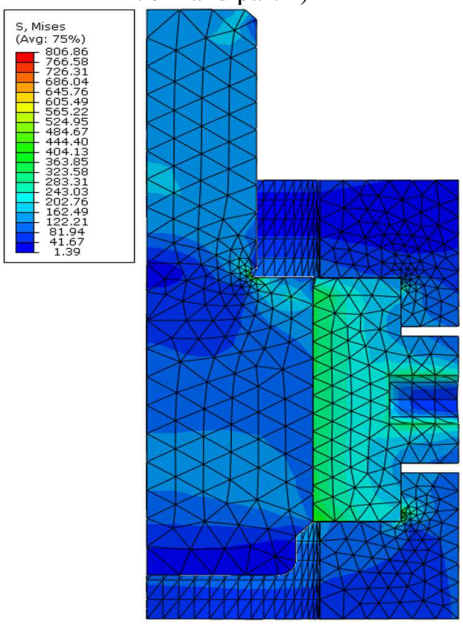

Fig. 14. Distribution of the equivalent von Mises stress at the level of the parts that make up the shrinkage assembly at an axial displacement of the hub of 50 mm (in the case of a friction coefficient , $\mu = 0.125$ on the contact surface between the hub 4 and part 2)

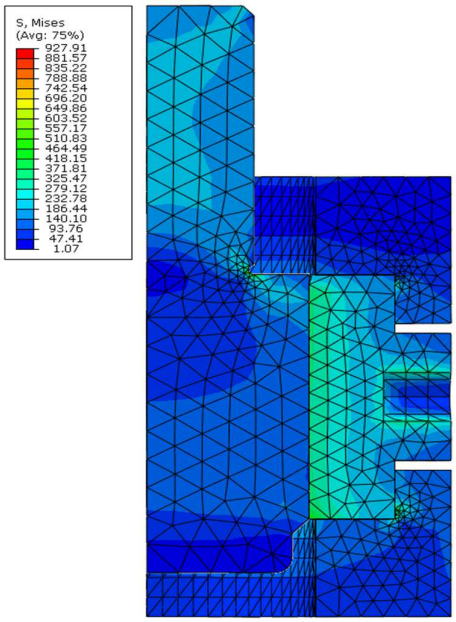

Fig. 15. Distribution of the equivalent von Mises stress at the level of the parts that make up the shrinkage assembly at an axial displacement of the hub of 50 mm (in the case of a friction coefficient μ = 0.150 on the contact surface between the hub 4 and part 2)

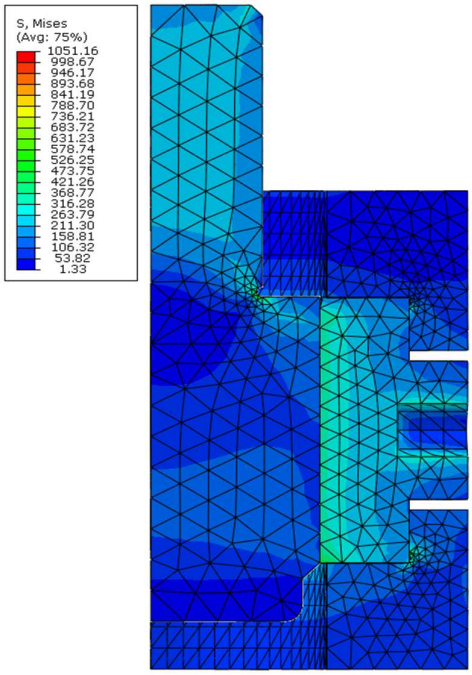

Fig. 16. Distribution of the equivalent von Mises stress at the level of the parts that make up the shrinkage assembly at an axial displacement of the hub of 50 mm (in the case of a friction coefficient μ = 0.175 on the contact surface between the hub 4 and part 2)

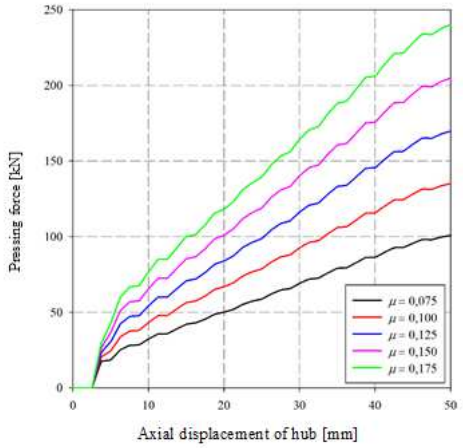

Fig. 17 Evolution of the pressing force developed by the turntable 5 as a function of the axial displacement of the hub 4, for different values of the friction coefficient on the contact surface between the hub 4 and the piece 2

The evolutionary curves in Figure 17 are also consistent with expectations under the following respects:

- The appearance of the curves remains ascending, regardless of the level of friction between the hub 4 and the part 2. This can be explained by the extension of the contact surface with the vertical movement of the hub.
- Increasing the friction coefficient causes higher and higher values of the maximum pressing force developed by the turntable 5.

Table 3 shows the maximum values of the pressing force developed by the turntable 5 for different values of the friction coefficient associated with the contact surface between the hub 4 and the piece 2. The numerical data in this table are represented graphically in figure 18.

Table 3. Dependence of the maximum values of the pressing force developed by the turntable 5 on the level of friction on the contact surface between the hub 4 and the piece 2.

Friction coefficient associated with the contact surface between the hub 4 and the piece 2 μ [-]	The pressing force developed by the turntable 5 F_{max} [kN]
0.075	100.78
0.100	135.16
0.125	169.83
0.150	204.84
0.175	240.23

The diagram in Figure 18 describes a practically linear dependence between the maximum pressing force F_{max} and the friction coefficient μ associated with the contact between the hub 4 and part 2. This dependence is very well approximated by the regression

$F_{max}(\mu) = 1394{,}3616 \cdot \mu - 4{,}1266$ [kN], for $0{,}075 \leq \mu \leq 0{,}175$ (1)

By reversing the relation (1) its dependence is obtained the dependence of μ on F_{max}:

$\mu(F_{max}) = 7{,}1717 \cdot 10^{-4} \cdot F_{max} + 29{,}5949 \cdot 10^{-4}$[-], for $100 \text{ kN} \leq F_{max} \leq 240 \text{ kN}$. (2)

The formula (2) can be used to determine the best calculation value of the friction coefficient μ, when the maximum value of the pressing force F_{max} is known (for example, a value of the force determined by laboratory tests).

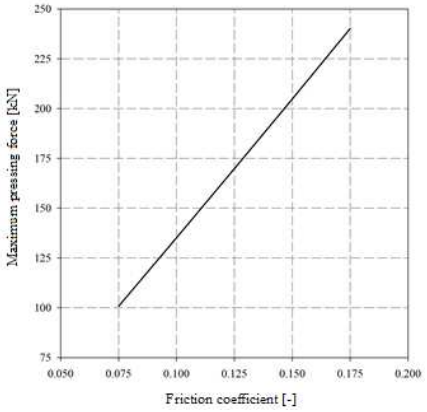

Fig. 18. Dependence of the maximum values of the pressing force that the turntable 5 develops on the level of friction on the contact surface between the hub 4 and the piece 2

Obviously, the relations (1) and (2) are valid exclusively for the case of the shrinkage assembly in figure 1. They must not be extrapolated in the case of parts of other shapes or dimensions. Also, the validity of the relations (1) and (2) is only guaranteed in the ranges $0.075 \leq \mu \leq 0.175$ and $100 \text{ kN} \leq \text{Fmax} \leq 240$ kN, intervals for which these formulas were determined by the linear regression of the numerical data from the table 3.

3. EXPERIMENTAL RESEARCH

3.1 Introduction

Experimental research was performed in order to define the shrinkage process using the finite element method in the field of computer aided design of shrink assembly.

The layout of the shrink assembly under analysis is shown in Figure 1. The process is considered to take place at the room temperature and involves the forced insertion of the hub 4 into the bore of part 2 (Fig. 1).

The parts shown in figure 1 are made of the following materials: alloy tool steel X210CrW12 (SR EN ISO 4997: 2018) in the case of part 2 and hub 4, respectively non-alloy steel for hardening and tempering C45 (SR EN ISO 10088-2: 2007) in the case of rings 1 and 3 (fig. 1).

The finite element analysis of the shrinkage process was performed assuming an elastic behavior of all parts shown in Figure 1. Table 1 shows the elastic parameters of the two steels from which the parts are made (Young's modulus and Poisson's ratio).

The pressing of the two parts was performed on a machine for static testing of metals at traction and compression type WEW - 600D, maximum force 600 kN. The pressing speed must not exceed 5 mm / s [9].

3.2 Elastic tightening assembly using dry surfaces

Depending on the size of the tightening, in the parts may occur elastic, elastic-plastic or plastic deformations.

Figure 19 shows the diagram of the variation of the pressing force depending on the length of the adjustment and time, having dry surfaces.

a)

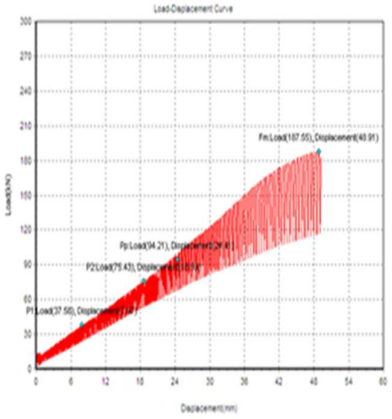

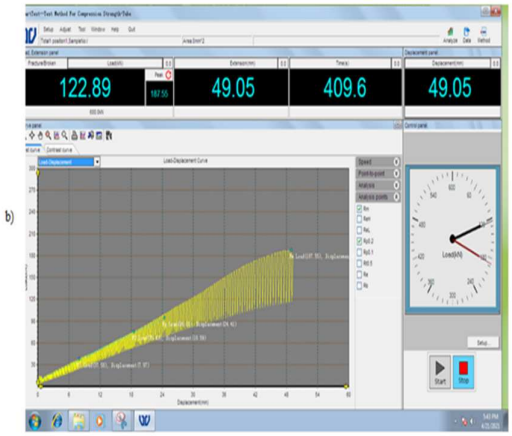

Fig. 19. Diagram of the variation of the pressing forces depending on: a) the length of the adjustment, l = 48.91 mm; b) pressing time, t = 409.6 s, cross beam speed was, v =0.12 mm / s, Fmax = 187.55 *kN*

Elastic tightening assemblies are usually included in the group of non-removable joints.

3.3 Elastic tightening assembly using oiled surfaces with Liqui Moly 10W40

The pressing force increases in proportion to the length of the pressing.

By lubricating the adjusted surfaces, the required axial force is reduced (fig. 20).

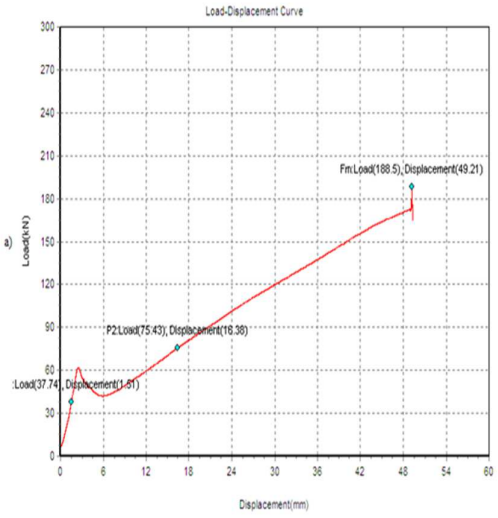

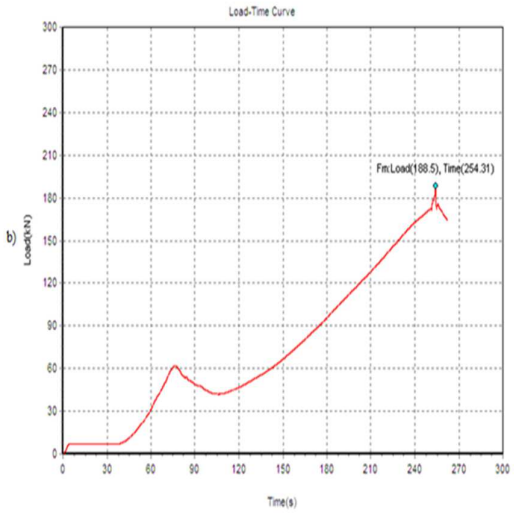

Fig. 20. Diagram of variation of pressing forces in case of lubrication the surfaces with Liqui Moly 10W40 oil depending on: a) length; b) time, v = 0.20 mm / s,

In this case the maximum pressing force Fmax = 188 kN, on the length l = 49.21 mm, for 254.6 sec, it is observed that the maximum force has decreased (see fig. 19), and the deformation of the adjustment at the beginning is elastic.

3.4 Assembly by elastic tightening using surfaces greased with additive oil, Liqui Moly oil

A direction for the development of fluid lubricants is to add to mineral oils small amounts of substances capable of changing their properties in the desired direction, or even giving them new properties. These substances are generally called additives. Liqui Moly 10W40 oil with molybdenum sulfide (MoS2) additive was used in the research.

Figure 21 shows the diagram of pressing forces in case of lubrication of surfaces with additive oil.

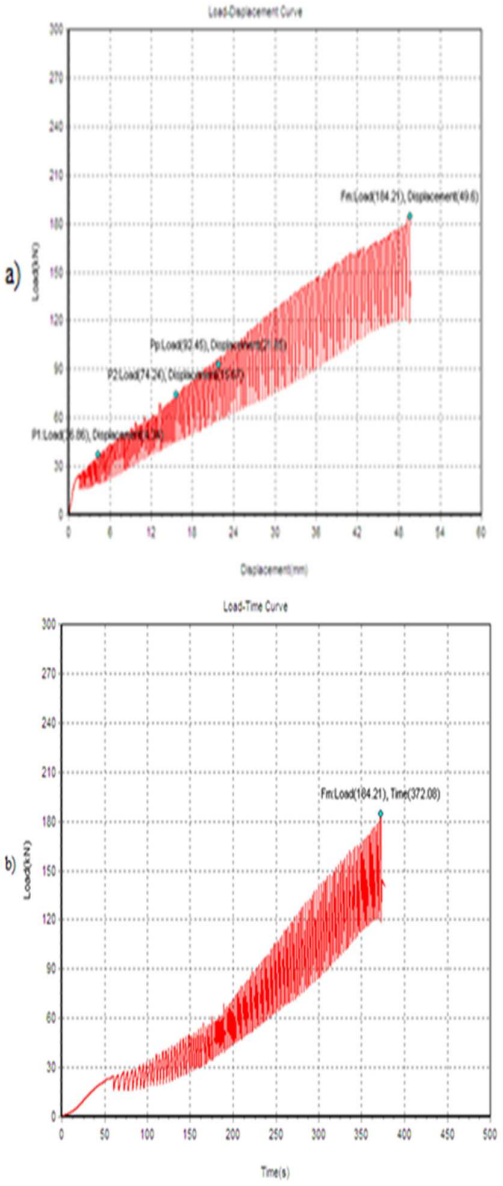

Fig. 21. Diagram of the variation of the pressing force in case of surface lubrication with additive oil: a) length, l = 49.6; b) time, t = 372.08 sec.

In this case the maximum pressing force F_{max} = 184.21 kN, it is observed that the maximum force has decreased (see fig. 20).

3.5 Elastic tightening assembly using surfaces greased with Vaseline

The lubrication of the adjusted surfaces was done with graphite Vaseline added with molybdenum.

By lubricating the adjusted surfaces, the required axial pressing force is reduced and the mounting in good condition is ensured.

Figure 22 shows the variation diagram of the pressing force, depending on the length of the adjustment and the time.

Like any adjustment, a pressed assembly is characterized by tightening and accuracy class, the latter actually expressing the size of the adjustment tolerances.

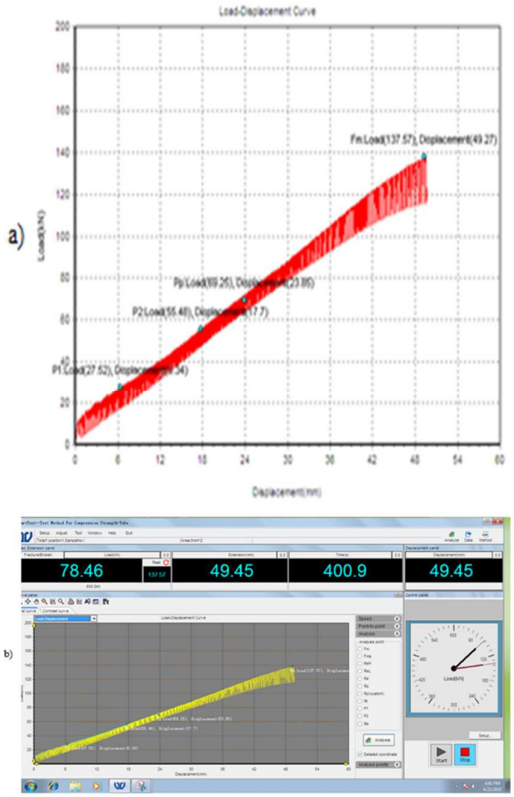

Fig. 22. Diagram of variation of the pressing force in the case of lubrication of the surfaces with Vaseline: a) length, l = 49.27 mm; b) time, t = 400.9 sec.

Comparing the maximum force in Figure 19 (F_{max} = 187.55 kN) with the pressing force in Figure 22 where F_{max} = 137.57 kN, a substantial decrease in the pressing force is found.

Longitudinal pressing is performed by means of a machine for static testing of metals at traction and compression, having the maximum pressing force F_{max} = 600 kN, type WEW - 600D (fig. 23).

It was found experimentally that the pressing force is also dependent on the pressing speed,

decreasing with increasing speed. However, it is recommended that this speed not exceed 5 mm/sec [11].

Fig. 23 Static metal testing machine for traction and compression type WEW - 600D

4. CONCLUSIONS

Quality influences the economic aspects of the company's activity in two fundamental ways:

- the effect on income;
- effects on cost.

Finding the right balance between the cost of quality and the value of quality is not an easy task as the influencing factors are scattered among the different departments or sections of the company, in the distribution network, at the supplier, at the beneficiaries, etc.

Whether the factors influencing the value of quality are difficult to detect. As is well known, there are currently two notions regarding the quality:

- project quality;
- quality of compliance.
-

The decisive problem in terms of the economic aspects of quality of compliance, is the level of defects existing in the different stages of manufacture, as well as in the delivered product.

The finite element method is currently the most widespread method of numerically solving engineering problems.

The main advantages of MEF are the following [8]:

- flexibility (by allowing the discretization of bodies of no matter how complex shape they have and the natural manipulation of the most diverse borderline conditions;
- the possibility to model inhomogeneous bodies in terms of physical properties;
- easy implementation in general computer programs.

The most important disadvantage of MEF is the large volume of input data required for the construction and numerical solving of the model.

Experimental research has an important weight in scientific research, which is on the one hand a basic criterion for verifying the truth about the hypotheses of scientific theories, and on the other hand a source of finding new knowledge in the field studied.

Analyzing the evolution of the pressing force for different values of the coefficient of friction on the contact surface determined by MEF shown in figure 4.17 and the evolution of the pressing force determined by practical tests and presented in figures 5.1…..5.4 there is a practically linear dependence between the maximum pressing force F_{max} and the friction coefficient "μ".

5. REFERENCES

[1] [Aba2011a]. *** Abaqus Analysis User's Manual, Version 6.11-3 (documentation in electronic format). Providence: Abaqus, Inc., 2011

[2] [Aba2011b]. *** Abaqus/CAE User's Manual, Version 6.11-3 (documentation in electronic format). Providence: Abaqus, Inc., 2011

[3] [Aba2011c] *** Abaqus/Viewer User's Manual, Version 6.11-3 (documentation in electronic format). Providence: Abaqus, Inc., 2011

[4] Buzdugan, Gh. Resistance of materials, Technical Publishing House, Bucharest, 1970

[5] Buzdugan, Gh. Resistance of materials, Technical Publishing House, Bucharest, 1980

[6] Cândea, v.ș.a Classification and symbolization of ferrous and non-ferrous alloys, UT-PRESS Publishing House, Cluj-Napoca, 2010

[7] Chișu, Alex, ș.a. Machinery Parts, E.D.P. Publishing House, Bucharest 1976

[8] Comșa, Dan-Sorin, Finite elements method. UTPRESS, Cluj-Napoca 2007

[9] Deutsch, I. Resistance of materials, E.D.P. Publishing House, Bucharest, 1976

[10] Drăghici, I., ș.a. Machinery Parts, Problems, E.D.P. Publishing House, Bucharest, 1980

[11] Manea, Gh. Machinery Parts, Technical Publishing House, Bucharest, 1970

[12] Păstrăv, I. Resistance of materials, Vol. 2, I.P.C-N. Publishing House, Cluj-Napoca, 1983

[13] Tăpălagă, I. ș.a. Cold Extrusion of Metals, Dacia Publishing House, Cluj-Napoca, 1986

[14] Tăpălagă, I. ș.a. Cryogenics in the Machine Building, Dacia Publishing House, Cluj-Napoca, 1988.

REZOLVAREA NUMERICĂ A PROBLEMELOR INGINEREŞTI PRIVIND ÎMBINĂRILE CU STRÂNGERE ELASTICĂ

REZUMAT: Metoda elementului finit este în prezent cel mai răspândit proces de rezolvare numerică a problemelor de inginerie. Atunci când se aplică MEF, domeniul ocupat de sistemul fizic analizat este discretizat în subdomenii de dimensiuni finite, delimitate de limite rectilinii sau curbilinii. Prin această operație, sistemul real este înlocuit cu o rețea de așa-numite elemente finite.

Prin aplicarea MEF obținem un sistem de ecuații care se rezolvă numeric în raport cu valorile nodurilor necunoscute. Principalele avantaje ale MEF sunt următoarele: flexibilitatea (permițând discretizarea corpurilor de orice formă complexă); posibilitatea de a modela corpurile neomogene din punctul de vedere al proprietăților fizice; implementare ușoară în programele de calculator generale. Cel mai important dezavantaj al MEF este volumul mare de date de intrare necesare pentru construcția și rezolvarea numerică a modelului.

Cristian-Ioan INOAN, PhD Student, Eng.: Technical University of Cluj – Napoca, Department of Manufacturing Engineering, 103 – 105 Muncii Blvd. 400641 Cluj – Napoca, E-mail: cristi-inoan@gmail.com Phone: 0040-745 128 412.

Radu-Nicolae CORCHEŞ, PhD Student, Eng.: Technical University of Cluj – Napoca, Department of Manufacturing Engineering, 103 – 105 Muncii Blvd. 400641 Cluj – Napoca, E-mail: radu-corcheș@delgaz-grid.ro Phone: 0040-744 644 515

Gheorghina RUS, PhD Student, Eng.: Technical Univeristy of Cluj, Școala doctorală, E-mail: ginarus67@gmail.com, Phone: 0744 – 667 542

Gheorghe ACHIMAŞ, Prof. PhD, Eng.: Technical University of Cluj – Napoca, Department of Manufacturing Engineering, 103 – 105 Muncii Blvd. 400641 Cluj – Napoca, E-mail: Gheorghe.Achimaș@tcm.utcluj.ro Phone: 0040 – 264 401 731